PCCP

Accepted Manuscript

www.rsc.org/pccp

Conformational Preferences of Monohydrated Clusters of the Imidazole Derivatives Revisited

Aditi Bhattacherjee[#] **and Sanjay Wategaonkar***

Department of Chemical Sciences, Tata Institute of Fundamental Research, Homi Bhabha Road, Mumbai 400 005, India

 # Present address: Chemical Sciences Division, Lawrence Berkeley National Laboratory, 1 Cyclotron Road, Berkeley, California 94720, United States

Submitted to

AUTHOR EMAIL ADDRESS: abhattacherjee@lbl.gov, sanwat@tifr.res.in

Address for correspondence:

Sanjay Wategaonkar

Telephone: 91-22-2278-2259, Fax: 91-22-2278-2106, E-mail: sanwat@tifr.res.in

Abstract

We present the IR spectroscopic investigations of benzimidazole (BIM), N-methylbenzimidazole (MBIM), and their monohydrates (W_1) carried out in supersonic jet in the region of N-H, C-H, and O-H stretching fundamentals. The C-H stretching modes in the monomers were studied with the aim of identifying the C(2)H mode (C atom between the two N atoms in the imidazole moiety) which is known to play an important role as H-bond donor in enzymes and ionic liquids. The assignment was aided by quantum chemical calculations as well as the literature data on FTIR measurements in the matrix. The monohydrated clusters were investigated for a global comparison with previously reported conformations of hydrated imidazole and related derivatives in the gas phase, matrices, and He nanodroplets. The BIM-W_1 complex showed the presence of three conformers; an N-H···O bound conformer (A') and two O-H···N bound conformers, tilted towards the phenyl side (A) and imidazole side (B), respectively. Although both A' and B type conformers have been reported in the literature, our experiments identify a new conformer (conformer A) in gas phase for the first time which has also been reported in crystal structures of histidine containing proteins. The binding energies of the three conformers were found to be of comparable magnitude, with the N-H···O bound structure lying in between (~ 0.02 – 0.04 kcal mol^{-1}) the O-H···N bound ones at the counterpoise corrected (cp) MP2/ aug-cc-pVDZ level of theory. The formation of two distinct but closely related O-H···N bound conformers (A and B) was additionally confirmed by studying the MBIM-W_1 complex. Binding energies of the MBIM-W_1 conformers were found to be higher than the analogous BIM-W_1 conformers by 0.2 kcal mol^{-1} at the cp-MP2/ aug-cc-pVDZ level. The C(2)-H···O or π bound water structures were not observed in the beam for monohydrated clusters of either monomer. While QTAIM calculations predicted secondary stabilization in the A type conformer by a C(4)-H···O hydrogen bond, such an effect due to a possible C(2)-H···O interaction was not found for conformer B. Experimentally, however, no spectral evidence was found for either the C(4)-H···O or the C(2)-H···O interaction.

1) Introduction

Imidazole is the chromophore of histidine, which is a naturally occurring and essential amino acid. It has been implicated as an important ligand in many enzymatic reactions, most notably hydrolases and proteases.[1, 2] As part of the catalytic triad in these enzymes, the imidazole unit in histidine acts as a proton shuttle between the neighbouring acidic and nucleophilic amino acids. The C(2)-H group therein is seen to be hydrogen bonded to the carbonyl oxygen of the peptide backbone.[3] The imidazole group is also an important constituent of many ionic liquids and has wide applications in electrochemistry and biology.[4-13] It is an interesting molecule from the viewpoint of hydrogen bonding interactions due to the presence of multiple hydrogen bonding sites. Hydration of the imidazole moiety is believed to primarily involve its conventional hydrogen bonding sites,[14] with the N-H···O and O-H···N bound structures lying close in energy. In addition to the conventional N acceptor and N-H donor sites, it also possesses an activated C(2)-H and an aromatic π electron density which could play a role in hydrogen bonding. Because of the inherent multiple H-bond donating/accepting sites in this heterocyclic ring, several spectroscopic studies have been carried out to determine the microhydration structures of both neutral and protonated imidazole.[15-17] While both the N-H···O and O-H···N bound structures of imidazole have been observed in the matrix and He nanodroplet studies, a gas phase study of 4-phenylimidazole revealed an exclusively N-H···O bound conformer for its 1:1 complex with water.[14] However, FTIR measurements in supersonic jet suggested that the first water molecule prefers to act as a hydrogen bond donor to imidazole.[18]

Microscopic hydration of biomolecules is an important phenomenon from the point of view of its possible influence on their structure, dynamics and biological activity in aqueous medium.[19, 20] Because of the large number of solvent molecules involved in the condensed phase and their highly dynamic and inhomogeneous behavior, it is difficult to study such interactions in bulk at the molecular level. Preparation of stoichiometric clusters of a molecule with a chosen solvent in the cold, collision-less environment provided by a supersonic jet expansion is considered to be ideal for molecular level investigations since it allows these clusters to be probed in a size-selected manner. For this reason, the hydrated clusters of biomolecules or their model compounds have been extensively studied in the gas phase.[21-25]

Single (UV) and double resonance (IR-UV) techniques are well established laser based spectroscopic methods to study hydrogen bonding interactions in molecular beams.[26] These methods require the presence of a suitable UV chromophore. Since the S_1-S_0 excitation of imidazole is in the deep UV,[27] we have used imidazole fused with a benzene ring to shift its excitation to a wavelength region accessible by the standard rhodamine dyes without affecting its hydrogen bonding functionalities. This also serves the additional purpose of rendering the C(2)-H bond of interest a local oscillator which helps in the investigation of its specific role in hydration by IR spectroscopy (Figure S1). The present work aims at determining the global minimum structures of the 1:1 complexes of BIM and MBIM with water and comparing them with the other possible structures, and finally to arrive at a consensus with the existing literature on the minimum energy structures of the monohydrate of the imidazole moiety.

2) Methods:

2.1 Experimental Section

The vacuum chamber used for the experiments was recently built in our laboratory. It consists of two coupled cylindrical chambers (400 mm long, 250 mm ID), differentially pumped by two turbo molecular pumps (Pfeiffer HiPace 1200, 1330 l-s^{-1}) which were backed independently by two rotary pumps (Pfeiffer Penta 35). The first chamber housed the sample compartment and the pulsed nozzle (General valve; series 9) assembly. The LIF measurements were performed in this chamber with a photomultiplier tube (Hamamatsu IP28) mounted orthogonal to the molecular beam axis. The molecular beam was then guided into the second chamber through a 2mm skimmer. It was fitted with a time-of-flight mass spectrometer (TOFMS) consisting of 3 metal grids [repeller @ +3000V, accelerator @+1800V, and ground] configured in the Wiley-McLaren type arrangement for extraction of the ion packets formed upon photoionization into a 30 cm time-of-flight (TOF) tube with a channeltron (Dr. Sjuts Optotechnik GmbH; KBL25RS) mounted at the end. At the entrance of the TOF tube an Einzel lens assembly consisting of three pairs of semi-cylindrical segments was mounted to focus/ steer the ions onto the detector to maximize the signal. The PMT/channeltron output signal was digitized by a digital storage oscilloscope (LeCroy Waverunner 604Zi) interfaced with a PC for data acquisition using a homebuilt program. All the spectra reported in this work are an average of a minimum of four scans for an improved S/N ratio.

The BIM and MBIM (99% purity, Sigma Aldrich) samples were heated at 90ºC and 65ºC, respectively and the vapors seeded in helium gas were expanded through a pulsed nozzle. A 0.5% premix of H_2O vapor in helium was used to prepare the water clusters. An Nd^{3+}:YAG (Quantel YG781C, 10Hz, FWHM ~ 6ns) pumped dye laser (Quantel TDL70) served as the excitation laser while another Nd^{3+}:YAG (Quantel Brilliant, 10 Hz, FWHM ~ 5ns) pumped dye laser (Pulsare, Fine Adjustment) served as the ionization laser. The frequency doubled visible dye lasers were calibrated both by the optogalvanic method and by recording the etalon fringe spectrum. A $LiNbO_3$ IR optical parametric oscillator (IROPO, LaserSpec) with an intracavity etalon (~ 0.5 cm^{-1}) was used for recording the IR spectra. A KTP based IROPO (without etalon, bandwidth 5 cm^{-1}) was used to cover the spectral region where the $LiNbO_3$ absorbs (~3480-3510cm^{-1}). Photoacoustic spectra of water vapor (ambient), NH_3, and CH_4 (~ 25 torr each, filled in a gas cell operated at 1 atm) were recorded and compared with the reference lines provided in the HITRAN database[28] for calibrating the IR OPO in the regions of O-H (4000-3500 cm^{-1}), N-H (3500-3200 cm^{-1}) and C-H (3150-2900cm^{-1}) stretches, respectively. Typical IR pulse energies used in the experiment were ~ 1 mJ in the O-H and N-H regions and ~3 mJ in the C-H region (since CH has much weaker oscillator strength than OH or NH). The UV and IR beams were focused onto the molecular beam by a quartz lens (50 cm focal length) and a CaF_2 lens (60 cm focal length), respectively. They were spatially overlapped in a counter-propagating manner and temporally synchronized such that the IR pulse preceded the UV excitation pulse by ~ 50 ns. The temporal synchronization of the lasers was achieved by a delay generator (SRS DG-535).

2.2 Computational methods:

All possible conformations for the monohydrated clusters of BIM and MBIM were optimized at both DFT (B3LYP as well as dispersion corrected functionals such as M06-2X, LC-ωPBE and ωB97X-D) and MP2 methods using 6-311++G** and aug-cc-pVDZ basis sets. The optimized conformations were subsequently subjected to harmonic frequency calculations for comparison with the experiment. Quantum chemical calculations were carried out using the Gaussian 09 suite of programs.[29] The binding energies of the complexes were corrected for the zero point energy (ZPE) and basis set superposition error (BSSE).[30] In addition, the minimum energy structures corresponding to those observed in the experiment were re-optimized at the MP2 level using counterpoise (cp) corrected gradient in order to obtain more reliable frequencies and binding energies.

The quantum theory of atoms in molecules (QTAIM) was applied to the wavefunctions furnished by the ab initio calculations in order to determine the topological parameters at the bond critical point.[31] This was done using the AIM2000 suite of programs.[32] The localized natural bond orbitals of the individual molecular fragments in the hydrogen bonded complexes were also constructed in order to characterize the overlapping orbitals leading to the interaction. The NBO analysis was performed with NBO 5.0 to identify the interacting orbitals.[33, 34]

3) Results:

3.1 Molecular electrostatic potential energy surfaces

In order to assess the binding preferences in the parent molecules, the molecular electrostatic potential (MEP) surfaces were generated. Figure 1 shows the MEP surfaces of BIM and MBIM computed at the MP2/aug-cc-pVDZ level of theory. The red and blue shaded regions around the molecules indicate the electronegative and electropositive regions, respectively. The N-H bond in BIM is a strong H-bond donor whereas the N atom acts as an acceptor in both the molecules. In addition, the C(2)-H in BIM shows a weak electropositive region in its vicinity, suggesting that it may function as a hydrogen bond donor. Computational studies have shown that the C(2)-H···O bound imidazole-water complex is about 2.06 kcal mol^{-1} weaker than the water dimer and its strength cannot be undermined.[35] The MEP of MBIM also shows a blue smear between the C(2)-H and the methyl group, suggesting that it may act as a potential hydrogen bond donor.

3.2 Electronic excitation spectra (LIF and 2cR2PI)

Figures 2(a) and 3(a) show the LIF excitation spectra of BIM and MBIM monomers, respectively. The strong features appearing in each spectrum at 36022 cm^{-1} and 35595 cm^{-1} were assigned to their respective S_1-S_0 band origin (0-0) transitions. This was also confirmed by recording the mass-selected 2c-R2PI spectra of BIM and MBIM shown in Figures 2(d) and 3(c), respectively. Our result is in good agreement with the previously reported values for the band origin transition of BIM.[36, 37] When water was introduced in the buffer gas line, some new features appeared in the LIF spectra of both BIM (Figure 2b, c) and MBIM (Figure 3b). These have been marked A' to E and A to E in the respective figures.

The new peaks observed in the excitation spectra can be assigned to the singly and multiply hydrated clusters of the monomers; alternatively, these can also correspond to multiple conformers for the same cluster stoichiometry. To make conclusive assignments, the 2c-R2PI spectra of the BIM-W_1 and MBIM-W_1 complexes were recorded by gating their specific masses in the time-of-flight mass spectrum. These are shown in Figures 2(e) and 3(d), respectively. BIM-W_1 gave rise to one red shifted feature (A') at 35954 cm^{-1} and three other blue shifted features at 36126 (A), 36171 (B), and 36239 cm^{-1} (C) with respect to the band origin of the monomer. The peak C at 36239 cm^{-1} was due to fragmentation of the 1:2 water complex into the 1:1 mass channel. This was confirmed by IR spectroscopy and will not be discussed further in this article. Similarly, those marked D and E arose from higher clusters and will form the subject of a following article.

Thus, three conformers were found in the jet for the BIM-W_1 complex; one red-shifted by 68 cm^{-1} (A') and two others blue-shifted by 104 cm^{-1} (A) and 149 cm^{-1} (B). The peak positions are summarized in Table 1. It is interesting to note that the relative intensities of peaks A', A, and B were completely reversed in the 2c-R2PI spectrum compared to the LIF spectrum. This is because the conformers corresponding to the blue shifted features underwent extensive fragmentation upon photoionization due to their low stability in the excited state or perhaps in the cationic state. This was also confirmed by recording the action spectra of the BIM-water clusters by monitoring the monomer mass channel at various levels of water content as shown in Figure S2. Red (blue) shift in the electronic origin upon hydrogen bonding indicates that the complex is stabilized (destabilized) to a greater extent in the excited state compared to the ground state. Typically, for π-π* transitions (as is the S_0-S_1 transition for BIM),[38, 39] the band origins for the complexes are red-shifted whenever the UV chromophore donates H-bond whereas blue shifted band origins signify that the chromophore is H-bond acceptor. However, conclusive proof for the structures can only be obtained from IR spectroscopy. It must also be mentioned here that the peaks A', A, B, and C were also observed in an earlier report on the BIM-W_1 system.[37] The authors had assigned peak A' to the band origin transition of the N-H···O bound conformer and peaks A, B, and C to low frequency intramolecular/intermolecular vibrations of the complex based on computed harmonic frequencies and comparison with the phenol-$(H_2O)_1$ data. However, these assignments turn out to be erroneous; A', A, and B represent three different conformers of the BIM-W_1 complex which will be apparent when we discuss the IR data.

The 2c-R2PI spectrum of MBIM-W_1 showed two features at 35712 cm^{-1} (A) and 35788 cm^{-1} (B), which were blue-shifted from the band origin of the monomer by 117 cm^{-1} and 193 cm^{-1}, respectively (Table 1). Since MBIM shares the same hydrogen bonding functionalities as BIM with an exception of the N-H donor which is methylated, it is apparent that the A' peak in the excitation spectrum of BIM-W_1 possibly originates from the N-H···O bound complex. The MBIM-W_1 complex was found to be much more stable upon photoionization compared to BIM-W_1, which is evident from the strong signals obtained for the A and B conformers in the R2PI spectra of MBIM-W_1 compared to BIM-W_1.

3.3 FDIR spectra

(a) BIM and MBIM

Before presenting the IR spectroscopic data of the water clusters, we discuss the IR spectra of the individual monomers. The spectra have been recorded in both the N-H (for

BIM) and C-H regions of the vibrational spectrum. While assignment of vibrational frequencies of bonds with high oscillator strength such as NH is fairly simple, it is not so straightforward for aromatic and aliphatic CH bonds, not only because of inherently weaker oscillator strength but also due to ubiquitous coupling with other CH stretch fundamentals or bend overtones. However, the C-H stretch region is spectroscopically important in the present context as it is implicated in the formation of hydrogen bonded complexes. Previous efforts by several groups to assign the C(2)H stretch in the imidazole group in various ionic liquids have shown marked difficulty because of Fermi resonances with combinations and overtones of ring vibrations.[40-42] Isotopic substitution and methylation at the C2 position were employed to interpret variations in peak intensities and unequivocally assert whether the structural motifs in imidazole based ionic liquids were governed by H-bonds or electrostatic interactions.[43-46] As the imidazole group is fused with a benzene ring in BIM and MBIM, the phenyl CH stretches are expected to appear in a spectrally distinct window compared to the C(2)H stretch. In addition the ring vibrations which complicate the analysis in case of ionic liquids will also be different in the present case compared to bare imidazole. Our assignments in the C-H region of BIM and MBIM are mainly based on results of quantum chemical calculations (Tables 2a-b, S1, and S2). These are also in good agreement with the previously reported FTIR data (Table 2a, b).

The C-H stretching normal modes of BIM are different from those of imidazole itself[47, 48] as illustrated by the normal mode eigenvectors shown in Figure S1. The C(2)H stretching mode is a local mode in BIM. Figure 4 shows the observed IR spectrum of BIM along with those computed at the B3LYP/aug-cc-pVDZ and MP2/aug-cc-pVDZ levels. The N-H stretch appeared at 3519 cm^{-1}, which is consistent with that reported for imidazole.[16] The frequencies computed at B3LYP and MP2 levels were scaled by 0.9634 and 0.9620 respectively to match the observed N-H frequency. Five C-H stretches are expected for BIM, one corresponding to the C(2)-H and four others for the C-H oscillators of the phenyl ring. Among the latter, the lowest frequency C-H stretching mode in the phenyl ring has very low IR cross-section and could not be observed in our experiment. The moderately strong stretches observed at 3080, 3068, and 3055 cm^{-1} were assigned to the CH stretching modes in the phenyl ring and were seen to agree well with the scaled computed frequencies (accounting for a systematic offset as different scaling factors may be required in the CH and NH regions) as well as with FTIR measurements in the Argon matrix (Table 2a).[49] Computationally, the C(2)-H stretching mode was predicted to be higher in frequency compared to the phenyl CH stretching modes. However, assignment of the C(2)-H was non-trivial, since its absorption cross-section is weak (as evident from the computed spectra) and two weak features were observed to the blue side of the phenyl CH stretching modes at 3095 and 3134 cm^{-1}. In order to make this assignment, the following exercise was carried out. The computed C(2)-H frequencies at the B3LYP, M06-2X, ωB97-xD, LC-ωPBE, and MP2 levels were corrected for the mean deviation of the scaled frequencies of the phenyl C-H stretching modes from those experimentally observed (see Table S1 for the details). This exercise predicted the C(2)-H frequency to be between 3096 to 3114 cm^{-1} at the DFT level (B3LYP, M06-2X, ωB97X-D, LC- ωPBE) and 3114-3122 cm^{-1} at the MP2 level. We therefore assign the frequency at 3095 cm^{-1} to the C(2)-H. FTIR spectrum of BIM recorded in an Ar matrix reported the C(2)-H frequency at 3093 cm^{-1}, which is in good agreement with our assignment.[49] The feature at 3134 cm^{-1} may be a combination band or a bend overtone.

Figure 5 shows the FDIR spectrum of MBIM along with those computed at the B3LYP and MP2/ aug-cc-pVDZ levels. The same scaling factors were used to obtain the stick spectra as those used for BIM. The transitions observed at 2968, 3004, and 3047 cm^{-1} are assigned to the CH stretching modes of the methyl group while those appearing at 3056, 3065 and 3077 cm^{-1} are assigned to the CH stretching modes of the phenyl ring. The latter set of frequencies is similar to those obtained in the case of BIM with the lowest frequency C-H normal mode of the six-membered ring being too weak to be observed. Assignment of the C(2)-H stretching mode was presented with the same difficulty as in BIM, i.e., two weak features were observed at 3103 and 3132 cm^{-1}. After correcting for the mean deviation of the scaled computed normal modes of the phenyl ring (Table S2), we assign the transition at 3103 cm^{-1} as the C(2)-H stretch. Computations at various levels predicted the phenyl CH stretches to be similar for both BIM and MBIM, whereas the C(2)-H stretch was predicted to shift to lower wavenumbers (~ 10 cm^{-1}) upon N-methylation. However, this frequency was observed to be 8 cm^{-1} higher for MBIM than the analogous assignment in BIM, in contrast to the computations. This discrepancy could be due to the use of the same scaling factor for both MBIM and BIM (due to the absence of any distinct marker such as NH frequency in the former) across the entire spectral range covering NH and CH stretches which possess different anharmonicities. Perhaps more sophisticated anharmonic calculations might be required to bridge this subtle gap between theory and experiment. It must be mentioned that reference 49 reports the C(2)-H stretching frequency at 3072 cm^{-1}; however, this number seems to be inconsistent as it offsets the phenyl CH stretches in BIM and MBIM by >10 cm^{-1} which are observed to be similar in the present work. This assignment is questionable mainly for two reasons; first, the peaks in the spectrum were not well-resolved and the scaling factors used for the assignment were not substantiated. The features appearing below 2950 cm^{-1} in the IR spectrum of MBIM (Figure 5) are most likely due to bend overtones or combination bands arising from anharmonic coupling. The peak assigned to the C(2)-H in both BIM and MBIM was split; it may be due to a Fermi resonance of the C(2)-H stretch with the overtone of the in plane C(2)-H bend. The feature observed at 3132 cm^{-1} in MBIM is analogous to the 3134 cm^{-1} peak observed in BIM and must have the same origin (i.e. either a combination band or a bend overtone), although at present it is unclear.

(b) BIM-W_1 and MBIM-W_1

The FDIR spectra of BIM-W_1 and MBIM-W_1 are shown in Figure 6 and Figure 7, respectively. The computed vibrational spectra (at the cp-MP2/aug-cc-pVDZ level) which best agree with the experimentally observed ones are also shown for comparison. They have been scaled by a uniform scaling factor of 0.9620, same as that used for the monomers. The corresponding equilibrium structures of the conformers inferred from the FDIR spectra are shown in Figure 8. The IR spectra computed on the counterpoise corrected surface are seen to match the observed spectra extremely well. To provide an insight into the refinement due to the cp correction, the IR spectra without any such correction are presented and discussed in the Supporting Information (Figure S3, S4 and Table S3).

The FDIR spectrum of the A' peak of the BIM-W_1 cluster shows a strong dip at 3408 cm^{-1} and two weak features at 3652 and 3748 cm^{-1}. The figure also shows the positions of the N-H stretch of BIM monomer and those of the symmetric and antisymmetric stretches of bare water molecule. It is obvious that the N-H stretching frequency of the BIM monomer is greatly red shifted (111 cm^{-1}) whereas the OH stretching frequencies of water are almost unshifted. Therefore the A' feature must be due to the N-H···O bound conformer. In the other two conformers (A and B), the N-H stretch was unaffected. The O-H stretching frequencies of water were shifted to 3465 and 3719 cm^{-1} in conformer A, and to 3475 and 3721 cm^{-1} in conformer B. The features at 3465 and 3475 cm^{-1} were assigned to the bound O-H groups and those above 3700 cm^{-1} were assigned to the free O-H groups. The red-shifts in the bound O-H frequency were 242 cm^{-1} and 232 cm^{-1} for conformer A and B, respectively, with respect to the central frequency of the symmetric and antisymmetric modes of water. This indicates that the water molecule in these conformers acts as a hydrogen bond donor. The higher FWHM for the bound O-H transition in B (8 cm^{-1}) compared to that in A (3 cm^{-1}) or the N-H···O bond in A' (4 cm^{-1}) was because of the higher bandwidth (5 cm^{-1}) of the KTP OPO used since $LiNbO_3$ absorbs in this region. The magnitudes of the O-H red shifts indicate that the water must be O-H···N bound, since O-H···π bonds appear in a characteristic frequency window of ~ 3600 cm^{-1} to 3650 cm^{-1}.[14, 50, 51] Computations revealed that these correspond to two energetically close conformers in which the water molecule is tilted either towards the phenyl side (A) or the imidazole side (B), conformer A being higher in energy by ~ 0.06 kcal mol^{-1} (Figure 8). No noticeable changes were registered in the positions or intensities of the peaks in the CH region of the conformers of the BIM-W_1 complex, showing that the CH modes are unaffected by the H-bonding interaction. A summary of the observed and computed stretching frequencies along with the assignment is provided in Table 3.

Since the hydrogen bond donating N-H is methylated in MBIM it can only be an acceptor in the MBIM-W_1 complex. The FDIR spectra of the MBIM-W_1 complex recorded by probing the electronic transitions labeled A and B gave two distinctly different hydrogen bonded O-H stretching frequencies, upholding the fact that they are different conformers. The bonded O-H stretches were obtained at 3454 and 3461 cm^{-1} while the free O-H stretches appeared at 3719 and 3721 cm^{-1}, respectively. The red-shifts in the bound O-H frequencies were 253 and 246 cm^{-1}, respectively, with respect to the central frequency of the symmetric and antisymmetric modes of water. The experimental spectra are best reproduced by structures similar to BIM-W_1 cluster where water acts as donor, i.e., with the water molecule tilted towards the phenyl side (A) and imidazole side (B), which are separated in energy by ~0.03 kcal mol^{-1}. Once again, no discernable changes in frequency or intensity were noted in the CH region of the spectrum in these conformers.

A few geometrical parameters relevant from the H-bonding point of view, the ZPE corrected binding energies, and the harmonic vibrational frequencies of the energy optimized conformers of BIM-W_1 and MBIM-W_1 observed in this work are provided in Table 4. In addition, the computed structures corresponding to those observed in our experiments were subjected to QTAIM calculations to find if they possessed any additional stabilizing influences other than the primary N-H···O or O-H···N hydrogen bonds. The molecular graphs obtained at the MP2/ aug-cc-pVDZ level of theory are shown in Figure S5. All the structures showed the presence of bond critical points along the hydrogen bond path with electron density and Laplacian of electron density values in the range accepted for hydrogen bonding.[52] The conformer A in both BIM-W_1 and MBIM-W_1 showed a BCP along the C(4)-H···O path and a ring critical point. However, the O-H···N bound conformer B did not show any BCP along the C(2)-H···O coordinate, suggesting that the C(2)-H bond does not have any secondary influence in the stability of this conformer. The values of the electron density and its Laplacian at the BCP have been provided in Table 4. They were within the accepted range for a hydrogen bonding interaction (0.002-0.040 au for ρ (r) and 0.024-0.139 au for $\nabla^2\rho$ (r)).[52] The NBO analyses were in agreement with these findings. The hydrogen bonding interactions are characterized by charge delocalization from the lone pair (LP) of the acceptor atom to the antibonding orbital (σ^*) of the donor X-H bond. Table 5 lists the interacting orbitals in all the conformers of the BIM-W_1 and MBIM-W_1 complexes and their associated second order perturbation energies obtained using the NBO analyses. The conformer A in both BIM-W_1 and MBIM-W_1 showed a weak secondary interaction due to the LP(2)O - σ^*(C4-H) overlap. No such secondary stabilization was found in the conformer B. Details of other equilibrium structures not observed in this work are given in the supporting information (Figure S6, Table S4).

In the conformers A and B (of both BIM and MBIM), the water molecule is tilted towards the phenyl C(4)-H side and the imidazole C(2)-H side, respectively. The QTAIM and NBO analyses rule out the C(2)-H···O interactions in the latter but predict small stabilization from the C(4)H···O interaction in the former. Therefore it is natural to question if it derives any stabilization from a secondary C(4)-H···O interaction. It must be noted that no evidence for such interactions was seen in the FDIR spectrum in the C-H region in terms of any shift or enhancement in the phenyl ring stretches. An O-H···N bound conformer with a more linear O-H-N bond angle was also optimized but it converged to either being tilted towards the imidazole or the phenyl ring at the MP2 level as well as the dispersion corrected DFT levels. It was found to be an equilibrium structure only at the B3LYP level; however its vibrational frequencies did not agree very well with the experiment (Figure S7, Table S5). A similar structure was also attempted for the MBIM-W_1 complex, but it converged to either A or B at both DFT (including B3LYP) and MP2 levels. The observed FDIR spectrum for this complex also did not show any evidence of secondary stabilization by either a C(2)-H···O or a C(4)-H···O hydrogen bond.

Previous investigations of the minimum energy structures of singly hydrated clusters of the imidazole moiety report widely different observations. While only an N-H···O bound structure was found in a study of 4-phenylimidazole[14], an FTIR study of bare imidazole in jet had evidence for only an O-H···N bound structure at low concentration of water.[18] Most FTIR studies in the matrix or in helium nanodroplet experiments, however, report an almost equal ratio of the two conformers based on their integrated intensities and relative energies.[16, 53] A summary of all the reports, along with the type of experiment and frequency shifts observed, is provided in Table 6. Interestingly, FTIR measurements on the 1:1 complexes of BIM and MBIM reported only a single O-H···N bound conformer (type B) in addition to an N-H···O bound conformer (for BIM).[49] The B type of isomer is the mostly widely reported O-H···N conformer for monohydrated imidazole/benzimidazole. This is the first report of the second, A type O-H···N bound conformer in BIM/MBIM. Though the QTAIM calculations predict secondary stabilization from the phenyl C(4)-H bond, *vide supra*, the possibility of such structure for imidazole-water complex cannot be out-rightly rejected. In fact the Cambridge Structural Database analysis of bound water molecules in the vicinity of an imidazole fragment in proteins clearly indicates both A and B as possible O-H···N bound conformers of the imidazole moiety.[54]

(c) Bend overtones:

The overtone of the O-H bending mode could be observed at high IR power (3 mJ) for the conformers A and B of both BIM-W_1 and MBIM-W_1. However, at low IR power (less than 1mJ which is the typical power under which the hydrogen bonded O-H stretches were measured) they were too weak to be observed. The overtone of the O-H bending mode of water for the O-H···N bound conformers of BIM-W_1 and MBIM-W_1 are shown in Figure 9. They appeared at 3201 and 3203 cm^{-1} for the conformer A of BIM-W_1 and MBIM-W_1, respectively, while for the conformer B they were observed at 3196 and 3199 cm^{-1}, respectively. These values are similar to those reported earlier, for example, in the case of the complexes of serotonin and 2-fluoropyridine with water.[23, 55] The O-H bending mode in water appears at 1595 cm^{-1} and the bend overtone appears at 3151 cm^{-1} for bare water in the vapor phase.[56] Figure 9 also shows the computed OH bend overtone frequency (obtained as two times the fundamental bend frequency scaled by 0.9703) of the assigned structures for comparison. The difference of 4-5 cm^{-1} in the relative positions of the OH bend overtones for the two types of conformers are very accurately reflected in the computed structures. Similar trends in the relative shifts in the electronic origin, fundamental O-H stretching mode and overtone of O-H bending mode in the BIM-W_1 and MBIM-W_1 complexes (A and B), support that they have closely related geometry.

4) Consensus with the existing literature

Ambiguity in the preferential site of attachment of a water molecule to imidazole, namely the O-H···N vs N-H···O conformer, remains unsettled despite the large body of work reported in the literature summarized in Table 6. These experiments have employed rather diverse experimental techniques as well as both unsubstituted and substituted imidazoles.[14, 16, 18, 49, 53] The observations differ widely from nearly equal ratio of the two conformers in cold matrices and He nanodroplets to exclusively one or the other in supersonic jet (albeit at low water concentration in ref 18). Quantum chemical calculations indicate a strong basis set dependence (Pople versus Dunning) of the relative energies of the two conformers. However, MP2 calculations with correlation consistent basis sets as well as coupled cluster computations predict higher stability of the O-H···N bound complex for bare imidazole, which has also been experimentally observed.[18] While relative conformational populations in a free supersonic jet are largely thermodynamically controlled, there is a greater degree of kinetic control in both matrices and nanodroplets.[57-60] Whether this is a sufficient reason to cause the different relative populations of N-H···O/O-H···N bound conformers in matrix/He nanodroplets (~1:1) compared to supersonic jet (1:0) is debatable.

The present work not only predicts isoenergetic water donor and acceptor conformers from quantum chemical calculations but also detects both of them experimentally. Moreover, it also reports two types of conformers (A and B type) of O-H···N bound conformers, which are not seen to be affected by methyl substitution at the N atom, as evidenced by both the fundamental H-bonded stretching transitions and bend overtones. From the electronic excitation spectra of BIM-W_1 and MBIM-W_1 complexes in our study, it is clear that the electronic origin of the O-H···N complex is significantly blue-shifted from that of the monomer (>100 cm^{-1}). This suggests that the water donor conformers of 4-phenylimidazole might also be similarly blue-shifted and hence may not have been detected in the previous study.[14] This conjecture is further upheld by FTIR measurements on jet-cooled 4-phenylimidazole-water cluster which gave evidence for much stronger signals corresponding to the water donor complex compared to the N-H···O conformer which had only a 'minor contribution'.[18]

Phenyl group is often used as a convenient UV chromophore to provide a fluorescent tag to the substrate of interest with the underlying assumption that it does not affect the nascent H-bonding propensities of the system under investigation. In this context, the experimental observation of different conformational preference of 4-phenylimidazole[14] compared to imidazole[18] with respect to binding of a water molecule is unclear. Imidazole is known to be a better base than acid[61] and it is important to investigate whether this trend is affected by chemical substitution. For this purpose, we optimized the structures of the N-H···O/ O-H···N bound conformers of imidazole and several related derivatives at the same level of theory used in this work (i.e., cp-MP2/aug-cc-pVDZ) and computed their binding energies. The test molecules included imidazole (IM), 4-methylimidazole (4MIM), 5-methylimidazole (5MIM), 4-phenylimidazole (4PHIM), 5-phenylimidazole (5PHIM) as well as the amino acid histidine (HIS). The optimized structures of all the monohydrated complexes are shown in Figure S8. Figure 10 shows a bar graph of the ZPE corrected binding energies of the N-H···O/ O-H···N bound conformers of imidazole and its aforementioned derivatives. The binding energies for the BIM-water complexes obtained from the present study are also included for comparison. It can be seen from the figure that the O-H···N conformer is predicted to be more stable than the N-H···O for almost all the complexes, with the exception of 5PHIM, in which the latter is marginally more stable due to an additional O-H···π H-bond (see Figure S8). The difference in the binding energies of the two types of conformers is lowest in the case of BIM (0.04 kcal mol^{-1}) and highest for methyl substituted imidazole (0.9 kcal mol^{-1}). It decreases in the order 4MIM/5MIM > IM > 4PHIM > HIS > BIM > 5PHIM and is consistent with the lower (higher) acidity of N-H and higher basicity of N upon methyl (phenyl) substitution. Thus, across all the imidazole derivatives investigated, the same trend was found for the relative stability of the O-H···N/N-H···O conformer (with an exception of 5PHIM) and no dramatic switch in the conformational preference was noted upon ring substitution. It therefore appears that both conformers of a singly hydrated imidazole group are close in energy (within 1 kcal mol^{-1}) with the former being marginally more stable for most cases. The difference between BIM and the other derivatives, however, was that while both A and B type of structures observed in this work were provided as input for possible O-H···N bound conformers, they were found to converge to one or the other at this particular level of theory.

5) Conclusion

The IR spectroscopy of BIM and MBIM and their 1:1 water clusters formed in supersonic jet was presented and discussed. Vibrational modes in the parent molecules were assigned by comparison with quantum chemical calculations as well as previously reported FTIR data. Both the N-H···O and O-H···N complexes were observed for the BIM-W$_1$ complex. In addition, the latter was found to exist as two conformations which differed in the orientation of the H-bond, being tilted either towards the five-membered imidazole ring or the six-membered phenyl ring. These two O-H···N bound conformers were also found for the MBIM-W$_1$ complex. While the C-H region of the vibrational spectra did not predict any involvement of the C(4)-H or the C(2)-H in stabilizing the A and B conformers, respectively, QTAIM calculations predicted the existence of a BCP along the C(4)-H···O bond path in conformer A. NBO analyses also showed occurrence of a weak charge delocalization from the lone pair of the O atom in H_2O to the antibonding orbital of the C(4)-H bond. This is the first report of the A type of conformer for the monohydrate of BIM and MBIM in the gas phase, which has also been reported earlier in the CSD analysis of imidazole in proteins.[54]

No evidence for the C(2)-H···O or O-H···π bound structures of the 1:1 water complex of BIM or MBIM was found in the jet.

The present results were also compared with monohydrated conformers of imidazole derivatives reported in the literature with regard to the donor/ acceptor dichotomy in this important and widespread biological molecule. The O-H···N and N-H···O conformers were very close in energy, with the former being marginally more stable, in line with the higher basicity of imidazole, and this trend is not expected to be affected upon chemical substitution. Our experimental results, corroborated by quantum chemical calculations, advance the understanding of the conformational preference of the side chain of histidine towards a single water molecule.

FIGURES

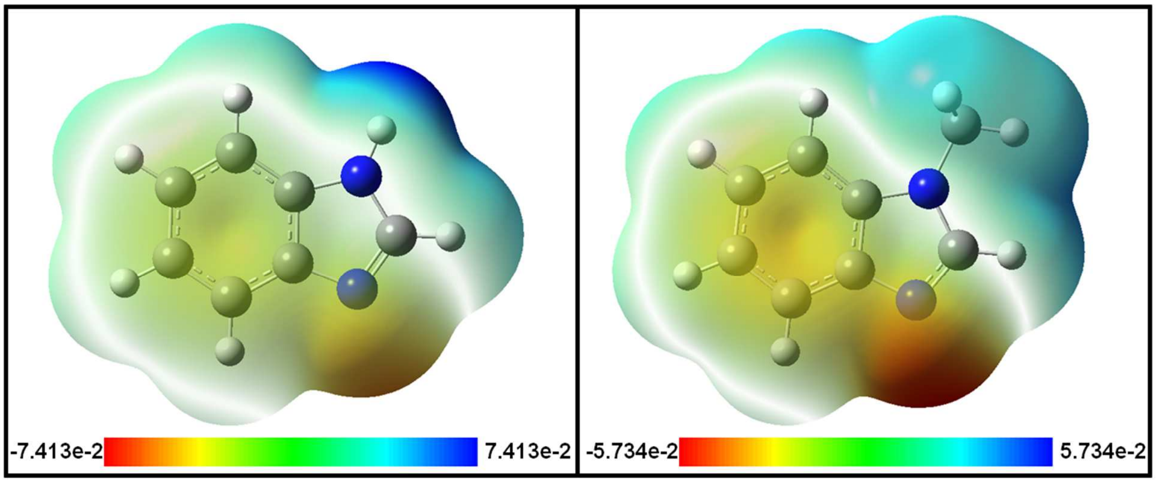

Figure 1: The molecular electrostatic potential (MEP) surface of BIM and MBIM computed at the MP2/ aug-cc-pVDZ level of theory at an isovalue electron density of 0.004 atomic units. The magnitudes of the MEPs (in atomic units) are depicted by the color bar at the bottom.

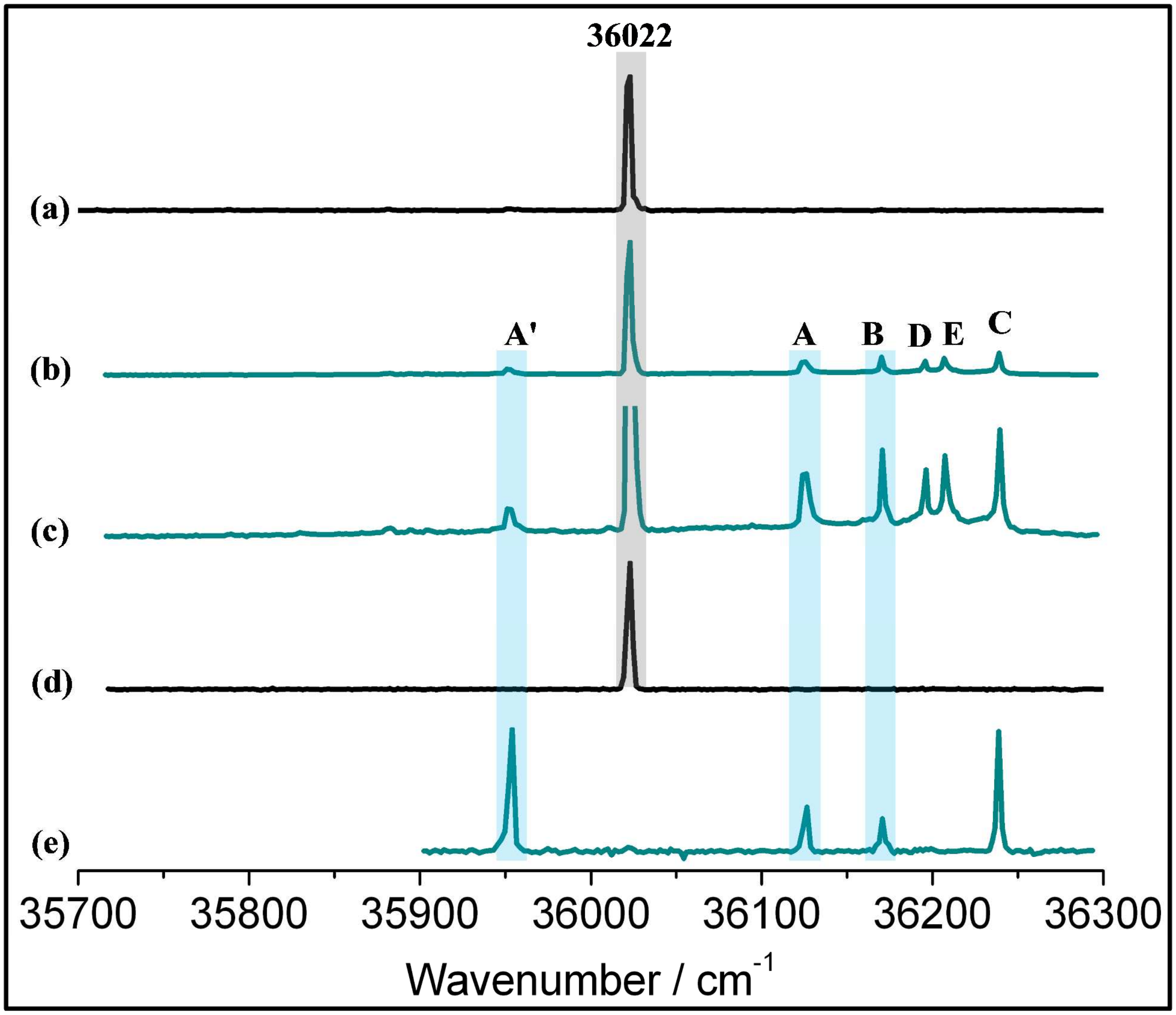

Figure 2: **(a)** LIF excitation spectrum of BIM. The S_1-S_0 band origin appears at 36022 cm^{-1}; **(b)** LIF excitation spectrum of BIM in presence of water shows several new features marked A' and A to E; **(c)** Zoomed trace (b); **(d)** 2c-R2PI spectrum of BIM monomer; **(e)** 2c-R2PI spectrum of BIM-W$_1$. The ionization laser was fixed at ~32785 cm^{-1}. Blue vertical bars are provided for assignment of the LIF features.

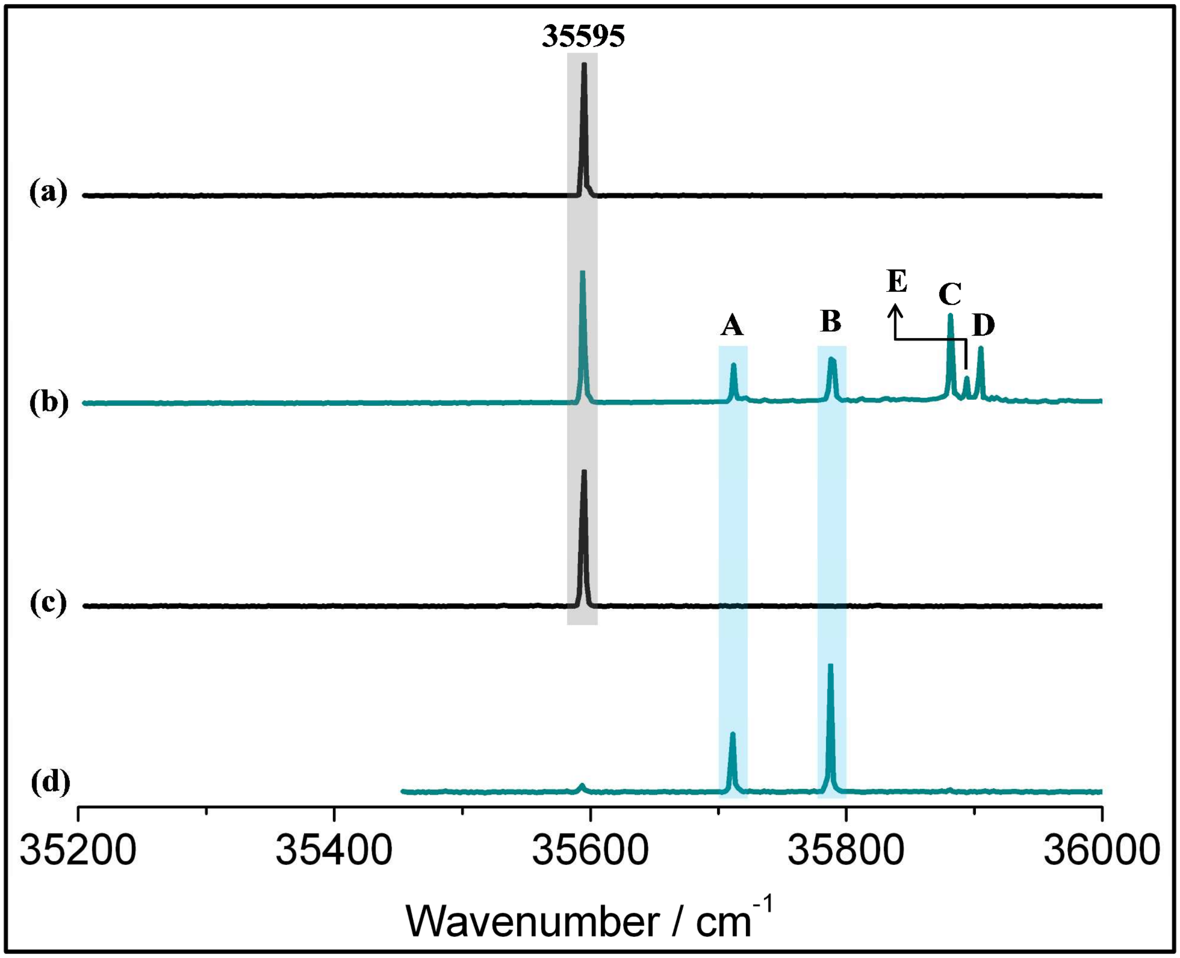

Figure 3: **(a)** LIF excitation spectrum of MBIM. The S_1-S_0 band origin appears at 35595 cm^{-1}; **(b)** LIF excitation spectrum of MBIM in presence of water shows several new features marked A to E; **(c)** 2c-R2PI spectrum of MBIM **(d)** 2c-R2PI spectrum of MBIM-W_1. The ionization laser was fixed at ~32260 cm^{-1}. Blue vertical bars are provided for assignment of the LIF features.

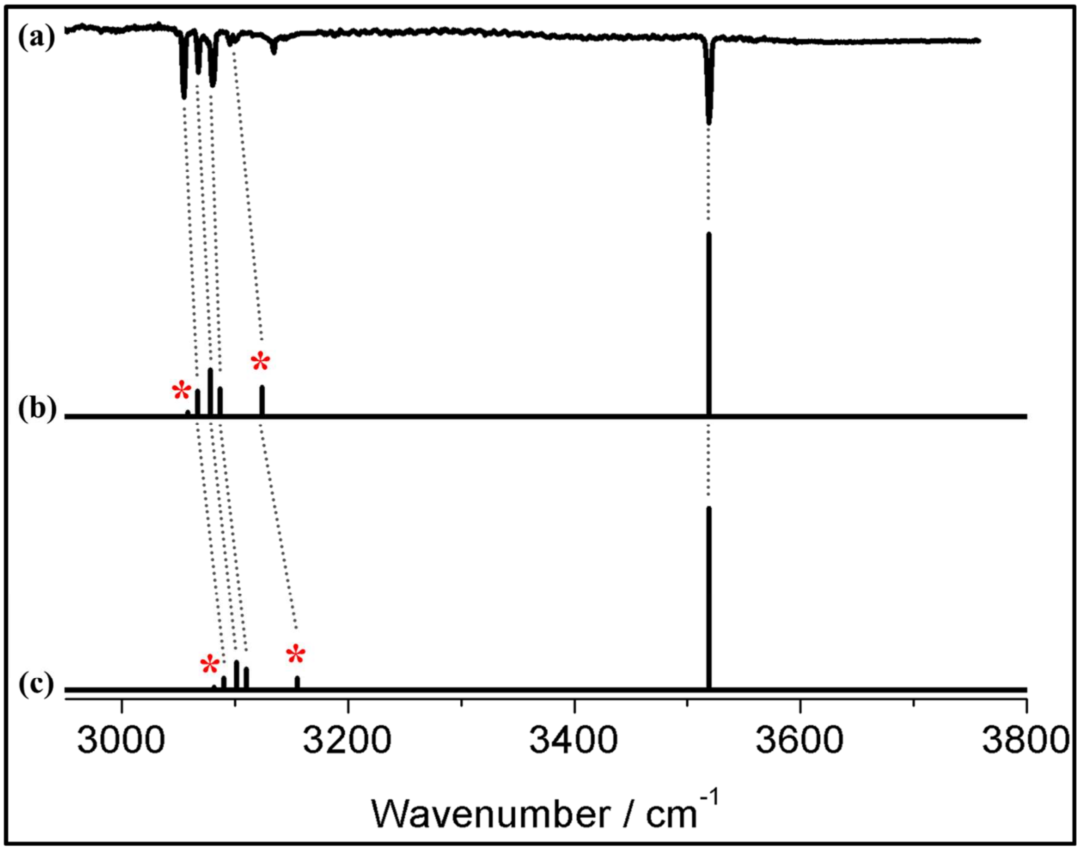

Figure 4: **(a)** FDIR spectrum of BIM obtained by setting the probe laser on the band origin transition at 36022 cm^{-1}; **(b)** Computed stick spectra at the B3LYP/aug-cc-pVDZ and **(c)** MP2/aug-cc-pVDZ levels were scaled by 0.9634 and 0.9620, respectively to match the NH transition. Gray dotted lines are provided to show the assignment (see Table 2(a) and text). Features marked * have been scaled in intensity by a factor of 10.

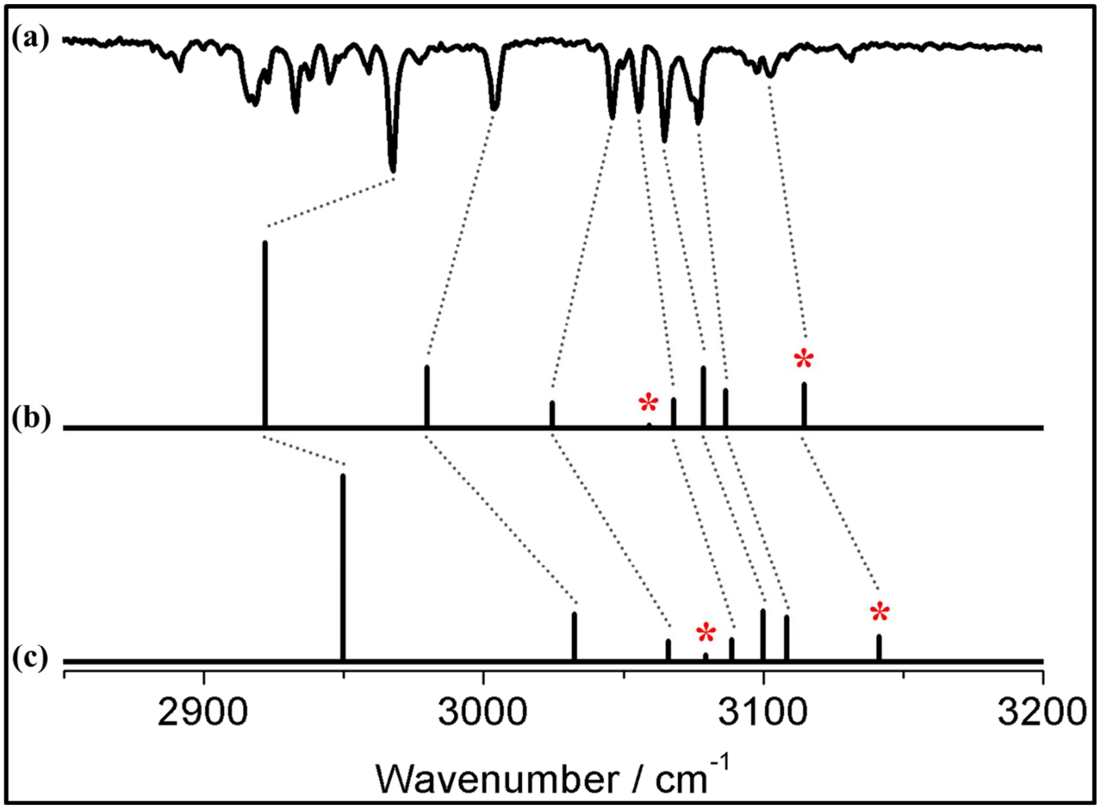

Figure 5: (a) FDIR spectrum of MBIM obtained by setting the probe laser on the band origin transition at 35595 cm^{-1}; **(b)** Computed stick spectra at the B3LYP/aug-cc-pVDZ and **(c)** MP2/aug-cc-pVDZ levels were scaled by 0.9634 and 0.9620, respectively. Gray dotted lines are provided to show the assignment (see Table 2(b) and text). Features marked * have been scaled in intensity by a factor of 10.

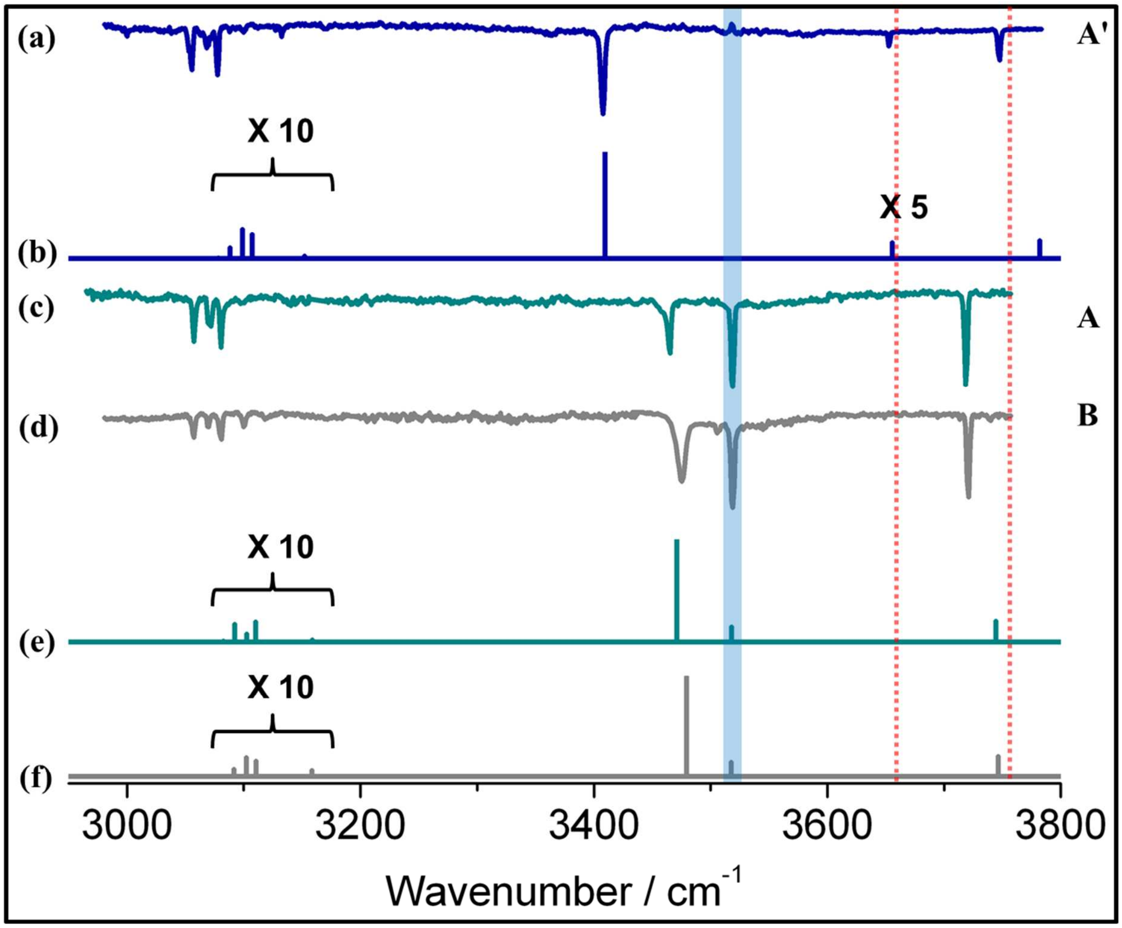

Figure 6: FDIR spectra of the BIM-W_1 complexes corresponding to the features in the electronic spectra [A' (trace a), A (trace c), and B (trace d), as indicated on the right]. The computed stick spectra at the cp-MP2/aug-cc-pVDZ level scaled by 0.9620 are shown for comparison. Weak features in the computed spectrum have been scaled in intensity by the factors indicated. The blue shaded vertical bar marks the position of the NH stretch in the monomer (3519 cm^{-1}) whereas the red dotted lines indicate the positions of the symmetric (3657 cm^{-1}) and antisymmetric (3756 cm^{-1}) stretches in bare water molecule.

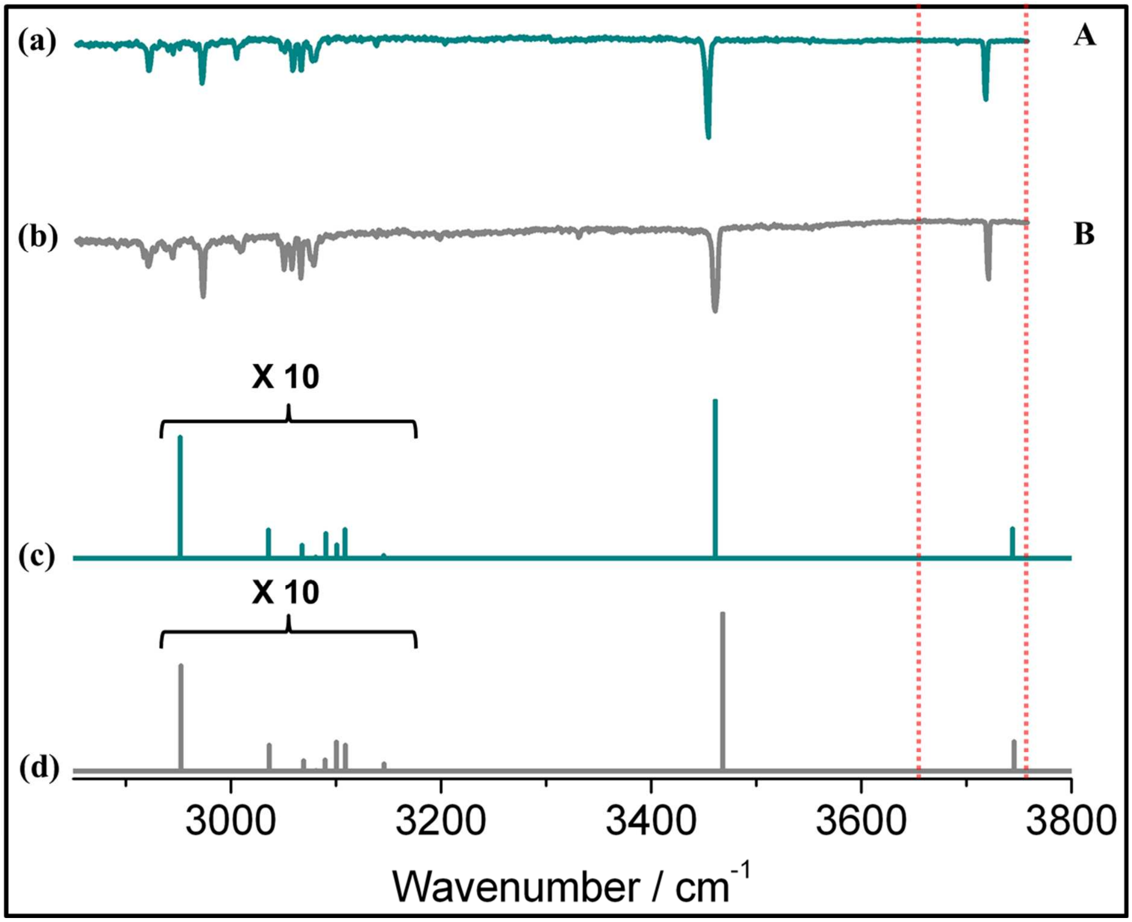

Figure 7: FDIR spectra of the MBIM-W$_1$ complexes corresponding to the features in the electronic spectra [A (trace a), and B (trace b), as indicated on the right]. The computed stick spectra at the cp-MP2/aug-cc-pVDZ level scaled by 0.9620 are shown for comparison. The CH frequencies in the computed spectrum have been scaled in intensity by a factor of 10. Red dotted lines indicate the positions of the free symmetric (3657 cm^{-1}) and antisymmetric (3756 cm^{-1}) stretches in bare water molecule.

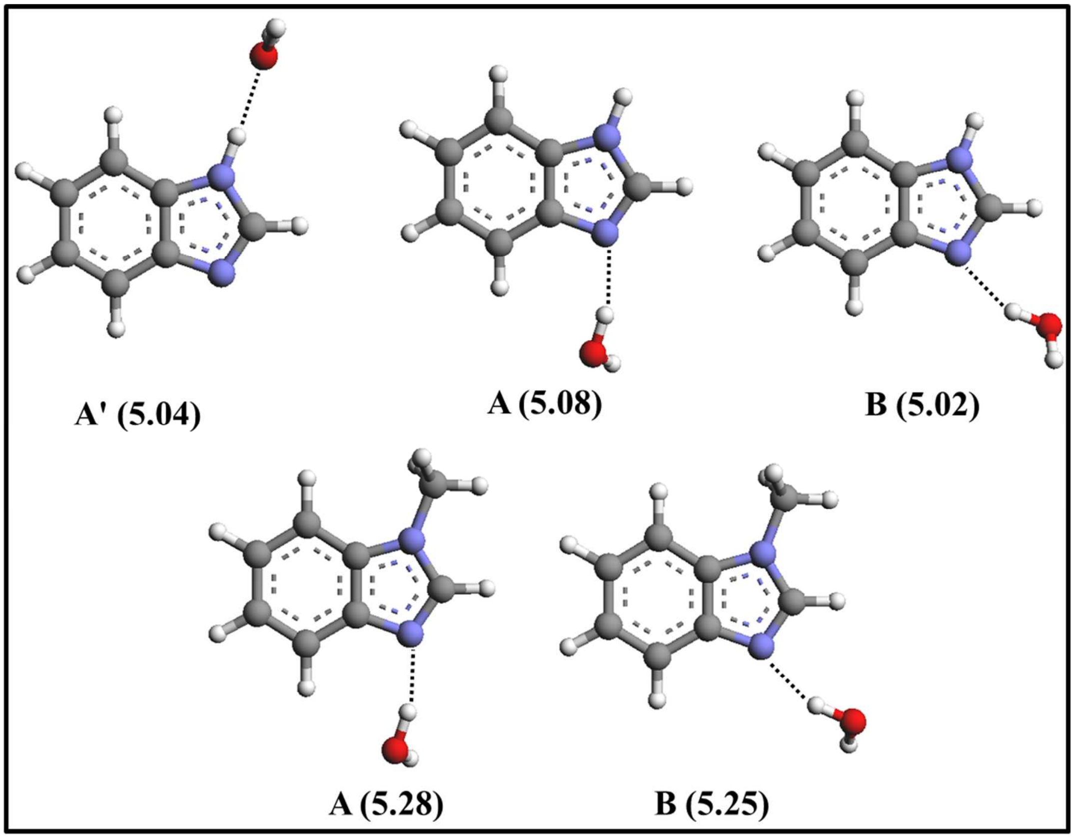

Figure 8: Optimized structures corresponding to the observed conformers of BIM-W_1 and MBIM-W_1 complexes at cp-MP2/ aug-cc-pVDZ level. Numbers in parentheses represent the binding energy in kcal mol^{-1}. For the other possible conformers of the monohydrated clusters and their binding energies, see the supporting information (Figure S6).

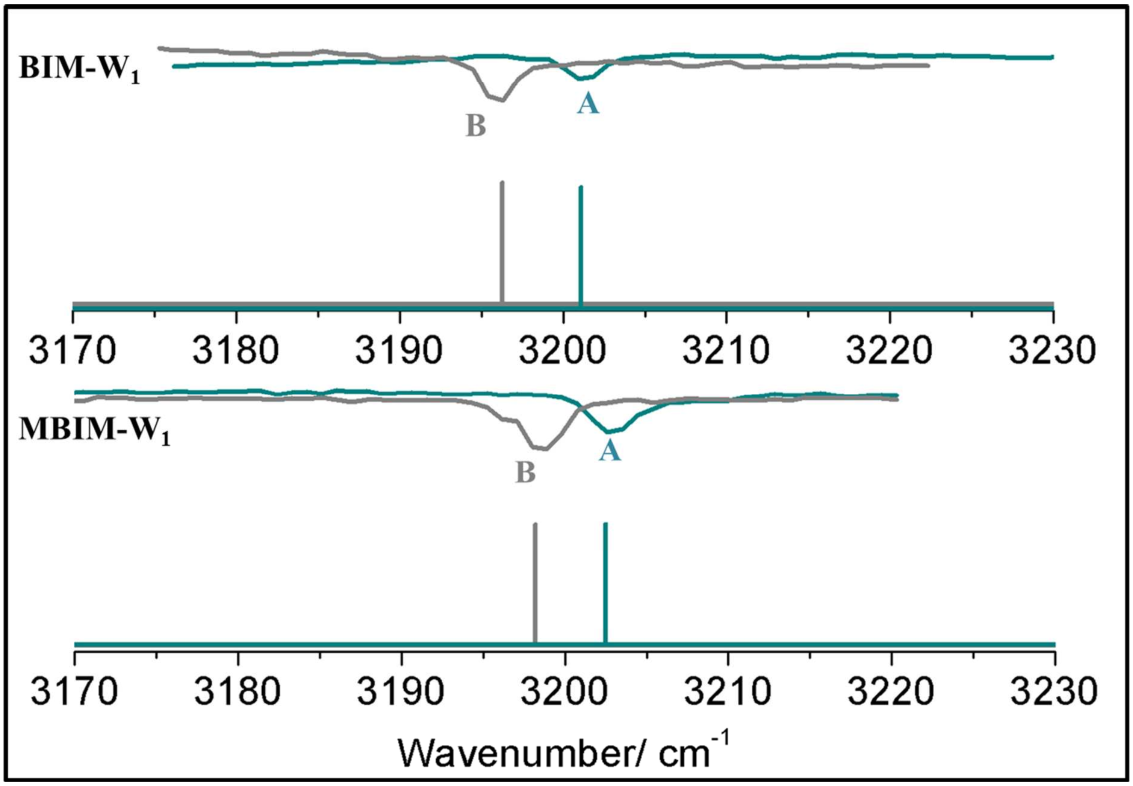

Figure 9: FDIR spectra recorded in the region of the overtone of the O-H bending mode at high IR power (3 mJ) for the conformers A and B of BIM-W_1 and MBIM-W_1. The computed frequencies (cp-MP2/aug-cc-pVDZ, scaled by 0.9703) corresponding to the two conformers are also shown for comparison.

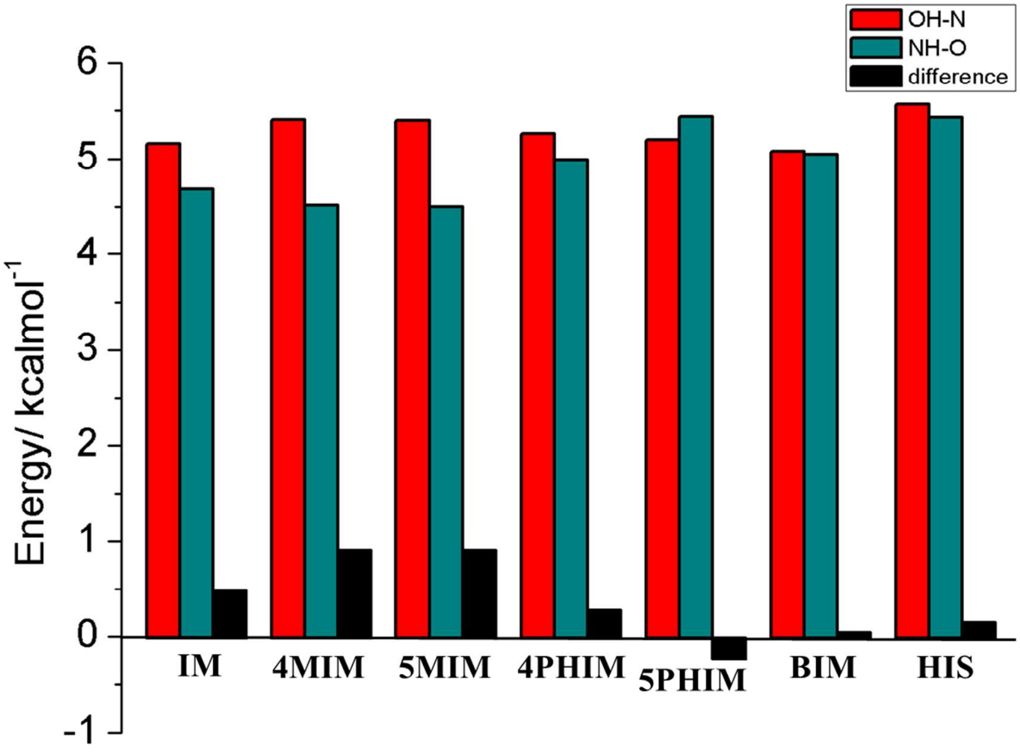

Figure 10: Binding energies of the O-H···N (red) and N-H···O (cyan) conformers of 1:1 water clusters of imidazole (IM), 4-methylimidazole (4MIM), 5-methylimidazole (5MIM), 4-phenylimidazole (4PHIM), 5-phenylimidazole (5PHIM), benzimidazole (BIM) and histidine (HIS). In case of BIM the more stable structure of the two O-H···N conformers (i.e. A) has been plotted. The black columns depict the difference in the binding energy between the two conformers (positive values are for more stable O-H···N compared to N-H···O).

Table 1: Positions (ν_{el}) and assignments of the transitions observed in the electronic spectra of BIM-W_1 and MBIM-W_1 clusters. $\Delta\nu_{el}$ denotes the shift in the 0-0 transition of the complex compared to that in the monomer (36022 cm^{-1} for BIM and 35595 cm^{-1} for MBIM).

Complex	Peak label	ν_{el} (cm^{-1})	$\Delta\nu_{el}$ (cm^{-1})
BIM-W_1	A'	35954	-68
BIM-W_1	A	36126	104
BIM-W_1	B	36171	149
MBIM-W_1	A	35712	117
MBIM-W_1	B	35788	193

Table 2(a): Experimental and computed frequencies (in cm^{-1}) for the N-H and C-H stretching modes of BIM and their assignments. Scaling factors of 0.9634 and 0.9620 were used at the B3LYP and MP2 levels, respectively. Columns 5 to 10 show comparison of the present work with FTIR measurements of BIM reported in the literature.

Experimentally Observed	Computed		Assignment	Ar matrix[49]	Ar matrix[62]	Solid/ KBr disc[63, 64]	Solid[65]	Crystal[66]	Solid[67]
	B3LYP/ aug-cc-pVDZ	MP2/ aug-cc-pVDZ							
3519	3519	3519	N-H	3508	3509	3460	--	--	3450
3134	--	--	*unassigned*	--	3124	--	--	--	--
3095	3124	3155	C(2)-H	3093	3095	3124	3115	3010s	--
3080	3087	3110	C-H, phenyl (1)	3076	3076	3104	3097	--	--
3068	3078	3101	C-H, phenyl (2)	3064	3065	3068	3065	3060s	3050
3055	3067	3090	C-H, phenyl (3)	3052	3052	3044	3040	--	--
—	3059	3081	C-H, phenyl (4)	--	--	3016	--	--	--

Table 2(b): Experimental and computed frequencies (in cm^{-1}) for the C-H stretching modes of MBIM and their assignments. Scaling factors of 0.9634 and 0.9620 were used at the B3LYP and MP2 levels, respectively. The last column shows comparison of the present work with FTIR measurements of MBIM in an Ar matrix.

Observed	**Computed**		**Assignment**	**Ar matrix**[49]
	B3LYP/aug-cc-pVDZ 0.9634	**MP2/aug-cc-pVDZ 0.9620**		
3132	--	--	*unassigned*	--
3103	3115	3141	C(2)-H	3072
3077	3087	3108	C-H, phenyl (1)	3060
3065	3079	3100	C-H, phenyl (2)	3051
3056	3068	3088	C-H, phenyl (3)	3041
—	3059	3079	C-H, phenyl (4)	3000
3047	3025	3066	C-H, methyl (1)	2955
3004	2980	3032	C-H, methyl (2)	2934/2928
2968	2922	2950	C-H, methyl (3)	2913

Table 3: Comparison of the experimentally observed fundamental stretching modes in the conformers of BIM-W_1 and MBIM-W_1 with those calculated at cp-MP2/ aug-cc-pVDZ. Calculated frequencies have been scaled by a uniform scaling factor of 0.9620. The assignment of the modes is provided in the last column. The C(2)-H stretch in the MBIM-W_1 conformers were too weak to be assigned.

BIM-W_1	**Observed**	**cp-MP2/ aug-cc-pVDZ**	**Assignment**
A'	3748	3782	O-H, antisymmetric
	3652	3656	O-H, symmetric
	3408	3410	Bound NH
	3100	3152	C(2)-H
	3078, 3068, 3056, —	3107, 3099, 3088, 3078(w)	C-H, phenyl
A	3719	3744	O-H, free
	3519	3518	N-H, free
	3465	3471	O-H, bound
	3097	3159	C(2)-H
	3081, 3072, 3057, —	3110, 3103, 3092, 3083(w)	C-H, phenyl
B	3721	3746	O-H, free
	3519	3518	N-H, free
	3475	3479	O-H, bound
	3100	3158	C(2)-H
	3081, 3069, 3057, —	3111, 3102, 3092, 3083(w)	C-H, phenyl
MBIM-W_1	**Observed**	**cp-MP2/ aug-cc-pVDZ**	**Assignment**
A	3719	3744	O-H, free
	3454	3461	O-H, bound
	—	3145	C(2)-H
	3078, 3067, 3059	3109, 3101, 3090, 3081(w)	C-H, phenyl
	3051, 3006, 2973, —	3068, 3036, 2952	C-H, methyl
B	3721	3745	O-H, free
	3461	3468	O-H, bound
	—	3146	C(2)-H
	3078, 3067, 3058	3109, 3101, 3090, 3081(w)	C-H, phenyl
	3051, 3009, 2974, —	3069, 3036, 2952	C-H, methyl

Table 4: Geometrical parameters, ZPE corrected binding energies, shifts in the XH stretching frequencies of the H-bond donor group, and electron density topological parameters of the optimized conformers of BIM-W_1 and MBIM-W_1 shown in Figure 8.

(# corresponds to BCP along C(4)-H···O).

Parameters	**BIM-W_1**			**MBIM-W_1**	
	A'	**A**	**B**	**A**	**B**
r(H···Y) (Å)	1.976	1.992	1.997	1.983	1.988
R(X···Y) (Å)	2.995	2.940	2.915	2.935	2.910
Δ X-H (mÅ)	6.73	12.19	11.76	12.74	12.38
∠X-H-Y (°)	177.4	162.7	155.4	163.6	156.4
R[C(2/4)-H···O] (Å)	—	2.753	2.955	2.791	2.982
D_0 (kcal mol^{-1})	5.04	5.08	5.02	5.28	5.25
$\Delta\nu_{X-H}$ (cm^{-1})	109	228	236	239	246
ρ_{H-Y} (au)	0.0232	0.0261/0.0069$^{\#}$	0.0259	0.0285/0.0071$^{\#}$	0.0273
$\nabla^2\rho_{H-Y}$	0.0996	0.1003/0.0269$^{\#}$	0.0993	0.0931/0.0251$^{\#}$	0.0900

Table 5: The NBOs involved in the hydrogen bonding interactions in the conformers of BIM-W_1 and MBIM-W_1 complexes and their second order perturbation energies in kcal mol^{-1}.

Complex	**Conformer**	**Interacting orbitals**	**Second order perturbation energy**
BIM-W_1	A'	LP(2)O— σ*(N1-H)	15.28
	A	LP(1)N3— σ*(O-H) LP(2)O— σ*(C4-H)	12.11 0.89
	B	LP(1)N3— σ*(O-H)	10.85
MBIM-W_1	A	LP(1)N3— σ*(O-H) LP(1)O— σ*(C4-H)	12.05 0.89
	B	LP(1)N3— σ*(O-H)	10.04

Table 6: Comparison of the IR spectroscopic data for the monohydrates of imidazole and its derivatives reported in this work and in previous experiments. All frequencies are reported in cm^{-1}. Frequency shifts are listed in parentheses. (IM corresponds to bare imidazole and 4PHIM corresponds to 4-phenylimidazole).

Conformer	**BIM-W$_1$**	**BIM-W$_1$**	**IM-W$_1$**	**IM-W$_1$**	**4PHIM-W$_1$**	**IM-W$_1$**	**Assignment**
	(this work)	**Ar matrix[49]**	**He nanodroplet[16]**	**Ar matrix[53]**	**Supersonic jet[14]**	**Supersonic jet[18]**	
A'	3748 (-8) 3652 (-5) 3408 (-111)	3724 (-12) 3632 (-6) 3358 (-150)	3747.7 — 3411.8	3725 (-11) 3632 (-6) 3373 (-127)	3747 (-9) 3656 (1) 3407 (-107)	—	O-H, antisym O-H, sym NH, bound
A	3721 (15) 3519 (0) 3475 (-232)	—	—	—	—	—	O-H, free N-H, free O-H, bound
B	3719 (13) 3519 (0) 3465 (-242)	3700 (-36) 3498 (-10) 3401 (-237)	3719.7 3517.8 3447.9	3702 (-34) 3503(+1) 3394 (-244)	—	-- -- 3458 (-248)	O-H, free N-H, free O-H, bound
Conformer	**MBIM-W$_1$**	**MBIM-W$_1$**					**Assignment**
	(this work)	**Ar matrix[49]**					
A	3721 (15) 3461(-246)	—	—				O-H, free O-H, bound
B	3719 (13) 3454 (-253)	3699 (-37) 3409/ 3400 (-229/-238)					O-H, free O-H, bound

References:

1 Z. S. Derewenda, U. Derewenda and P. M. Kobos, *Journal of Molecular Biology*, 1994, **241**, 83-93.

2 E. Erez, D. Fass and E. Bibi, *Nature*, 2009, **459**, 371-378.

3 E. L. Ash, J. L. Sudmeier, R. M. Day, M. Vincent, E. V. Torchilin, K. C. Haddad, E. M. Bradshaw, D. G. Sanford and W. W. Bachovchin, *Proceedings of the National Academy of Sciences of the United States of America*, 2000, **97**, 10371-10376.

4 B. C. Bae, H. Y. Ha and D. Kim, *Journal of the Electrochemical Society*, 2005, **152**, A1366-A1372.

5 I. V. Garist, S. P. Verevkin, J. E. Bara, M. S. Hindman and S. P. O. Danielsen, *Journal of Chemical and Engineering Data*, 2012, **57**, 1803-1809.

6 S. K. Kim, T. H. Kim, J. W. Jung and J. C. Lee, *Polymer*, 2009, **50**, 3495-3502.

7 K. Zhou and F. Zelder, *Angewandte Chemie-International Edition*, 2010, **49**, 5178-5180.

8 C. Mannel-Croise and F. Zelder, *Chemical Communications*, 2011, **47**, 11249-11251.

9 A. Fischer, H. Pettersson, A. Hagfeldt, G. Boschloo, L. Kloo and M. Gorlov, *Solar Energy Materials and Solar Cells*, 2007, **91**, 1062-1065.

10 L. L. Chang, K. L. Sidler, M. A. Cascieri, S. de Laszlo, G. Koch, B. Li, M. MacCoss, N. Mantlo, S. O'Keefe, M. Pang, A. Rolando and W. K. Hagmann, *Bioorganic & Medicinal Chemistry Letters*, 2001, **11**, 2549-2553.

11 P. P. Graczyk, A. Khan, G. S. Bhatia, V. Palmer, D. Medland, H. Numata, H. Oinuma, J. Catchick, A. Dunne, M. Ellis, C. Smales, J. Whitfield, S. J. Neame, B. Shah, D. Wilton, L. Morgan, T. Patel, R. Chung, H. Desmond, J. M. Staddon, N. Sato and A. Inoue, *Bioorganic & Medicinal Chemistry Letters*, 2005, **15**, 4666-4670.

12 D. C. Grills, Y. Matsubara, Y. Kuwahara, S. R. Golisz, D. A. Kurtz and B. A. Mello, *Journal of Physical Chemistry Letters*, 2014, **5**, 2033-2038.

13 L. Y. Sun, G. K. Ramesha, P. V. Kamat and J. F. Brennecke, *Langmuir*, 2014, **30**, 6302-6308.

14 F. O. Talbot and J. P. Simons, *European Physical Journal D*, 2002, **20**, 389-398.

15 M. R. Hockridge, E. G. Robertson and J. P. Simons, *Chemical Physics Letters*, 1999, **302**, 538-548.

16 M. Y. Choi and R. E. Miller, *Journal of Physical Chemistry A*, 2006, **110**, 9344-9351.

17 H. S. Andrei, N. Solca and O. Dopfer, *Chemphyschem*, 2006, **7**, 107-110.

18 J. Zischang, J. J. Lee and M. A. Suhm, *Journal of Chemical Physics*, 2011, **135**, 061102.

19 J. M. Sorenson, G. Hura, A. K. Soper, A. Pertsemlidis and T. Head-Gordon, *Journal of Physical Chemistry B*, 1999, **103**, 5413-5426.

20 K. Griebenow and A. M. Klibanov, *Journal of the American Chemical Society*, 1996, **118**, 11695-11700.

21 R. K. Sinha, S. Lobsiger, M. Trachsel and S. Leutwyler, *Journal of Physical Chemistry A*, 2011, **115**, 6208-6217.

22 N. J. Kim, H. Kang, G. Jeong, Y. S. Kim, K. T. Lee and S. K. Kim, *Journal of Physical Chemistry A*, 2000, **104**, 6552-6557.

23 T. A. LeGreve, W. H. James and T. S. Zwier, *Journal of Physical Chemistry A*, 2009, **113**, 399-410.

24 N. S. Nagornova, T. R. Rizzo and O. V. Boyarkin, *Science*, 2012, **336**, 320-323.

25 L. C. Snoek, R. T. Kroemer and J. P. Simons, *Physical Chemistry Chemical Physics*, 2002, **4**, 2130-2139.

26 T. Ebata, A. Fujii and N. Mikami, *International Reviews in Physical Chemistry*, 1998, **17**, 331-361.

27 D. S. Caswell and T. G. Spiro, *Journal of the American Chemical Society*, 1986, **108**, 6470-6477.

28 L. S. Rothman, I. E. Gordon, A. Barbe, D. C. Benner, P. E. Bernath, M. Birk, V. Boudon, L. R. Brown, A. Campargue, J. P. Champion, K. Chance, L. H. Coudert, V. Dana, V. M. Devi, S. Fally, J. M. Flaud, R. R. Gamache, A. Goldman, D. Jacquemart, I. Kleiner, N. Lacome, W. J. Lafferty, J. Y. Mandin, S. T. Massie, S. N. Mikhailenko, C. E. Miller, N. Moazzen-Ahmadi, O. V. Naumenko, A. V. Nikitin, J. Orphal, V. I. Perevalov, A. Perrin, A. Predoi-Cross, C. P. Rinsland, M. Rotger, M. Simeckova, M. A. H. Smith, K. Sung, S. A. Tashkun, J. Tennyson, R. A. Toth, A. C. Vandaele and J. Vander Auwera, *Journal of Quantitative Spectroscopy & Radiative Transfer*, 2009, **110**, 533-572.

29 G. W. T. M. J. Frisch, H. B. Schlegel, G. E. Scuseria, , J. R. C. M. A. Robb, G. Scalmani, V. Barone, B. Mennucci, , H. N. G. A. Petersson, M. Caricato, X. Li, H. P. Hratchian, , J. B. A. F. Izmaylov, G. Zheng, J. L. Sonnenberg, M. Hada, , K. T. M. Ehara, R. Fukuda, J. Hasegawa, M. Ishida, T. Nakajima, , O. K. Y. Honda, H. Nakai, T. Vreven, J. A. Montgomery, Jr., , F. O. J. E. Peralta, M. Bearpark, J. J. Heyd, E. Brothers, , V. N. S. K. N. Kudin, T. Keith, R. Kobayashi, J. Normand, , A. R. K. Raghavachari, J. C. Burant, S. S. Iyengar, J. Tomasi, , N. R. M. Cossi, J. M. Millam, M. Klene, J. E. Knox, J. B. Cross, , C. A. V. Bakken, J. Jaramillo, R. Gomperts, R. E. Stratmann, , A. J. A. O. Yazyev, R. Cammi, C. Pomelli, J. W. Ochterski, , K. M. R. L. Martin, V. G. Zakrzewski, G. A. Voth, , J. J. D. P. Salvador, S. Dapprich, A. D. Daniels, , J. B. F. O. Farkas, J. V. Ortiz, J. Cioslowski, and G. and D. J. Fox, Inc., Wallingford CT, 2010., *Gaussian 09, Revision C.01*, 2009.

30 S. F. Boys and F. Bernardi, *Molecular Physics*, 1970, **19**, 553-566.

31 R. F. W. Bader, *Chemical Reviews*, 1991, **91**, 893-928.

32 AIM 2000, *Version 2.0 ed.*, 2002.

33 F. Weinhold, *Journal of Computational Chemistry*, 2012, **33**, 2363-2379.

34 E. D. Glendening, J. K. Badenhoop, A. E. Reed, J. E. Carpenter, J. A. Bohmann, C. M. Morales and F. Weinhold, *Theoretical Chemistry Institute, University of Wisconsin, Madison*, 2001, NBO 5.0.

35 R. L. Ornstein and Y. J. Zheng, *Journal of Biomolecular Structure & Dynamics*, 1997, **14**, 657-665.

36 R. D. Gordon and R. F. Yang, *Canadian Journal of Chemistry*, 1970, **48**, 1722-1729.

37 C. Jacoby, W. Roth and M. Schmitt, *Applied Physics B-Lasers and Optics*, 2000, **71**, 643-649.

38 E. Cane, A. Trombetti, B. Velino and W. Caminati, *Journal of Molecular Spectroscopy*, 1991, **150**, 222-228.

39 G. Berden, W. L. Meerts and E. Jalviste, *Journal of Chemical Physics*, 1995, **103**, 9596-9606.

40 C. Roth, S. Chatzipapadopoulos, D. Kerle, F. Friedriszik, M. Lutgens, S. Lochbrunner, O. Kuhn and R. Ludwig, *New Journal of Physics*, 2012, **14**, 105026.

41 J. C. Lassegues, J. Grondin, D. Cavagnat and P. Johansson, *Journal of Physical Chemistry A*, 2009, **113**, 6419-6421.

42 J. Grondin, J. C. Lassegues, D. Cavagnat, T. Buffeteau, P. Johansson and R. Holomb, *Journal of Raman Spectroscopy*, 2011, **42**, 733-743.

43 C. J. Johnson, J. A. Fournier, C. T. Wolke and M. A. Johnson, *Journal of Chemical Physics*, 2013, **139**, 224305.

44 J. A. Fournier, C. T. Wolke, C. J. Johnson, A. B. McCoy and M. A. Johnson, *Journal of Chemical Physics*, 2015, **142**, 064306.

45 S. Cha, M. Ao, W. Sung, B. Moon, B. Ahlstrom, P. Johansson, Y. Ouchi and D. Kim, *Physical Chemistry Chemical Physics*, 2014, **16**, 9591-9601.

46 S. A. Katsyuba, E. E. Zvereva, A. Vidis and P. J. Dyson, *Journal of Physical Chemistry A*, 2007, **111**, 352-370.

47 S. T. King, *Journal of Physical Chemistry*, 1970, **74**, 2133-2138.

48 M. Cordesde and J. L. Walter, *Spectrochimica Acta Part A-Molecular Spectroscopy*, 1968, **A 24**, 237-252.

49 K. Schoone, J. Smets, L. Houben, M. K. Van Bael, L. Adamowicz and G. Maes, *Journal of Physical Chemistry A*, 1998, **102**, 4863-4877.

50 J. R. Carney, F. C. Hagemeister and T. S. Zwier, *Journal of Chemical Physics*, 1998, **108**, 3379-3382.

51 E. G. Robertson, *Chemical Physics Letters*, 2000, **325**, 299-307.

52 U. Koch and P. L. A. Popelier, *Journal of Physical Chemistry*, 1995, **99**, 9747-9754.

53 M. K. VanBael, J. Smets, K. Schone, L. Houben, W. McCarthy, L. Adamowicz, M. J. Nowak and G. Maes, *Journal of Physical Chemistry A*, 1997, **101**, 2397-2413.

54 G. Alagona, C. Ghio, P. Nagy, K. Simon and G. Narayszabo, *Journal of Computational Chemistry*, 1990, **11**, 1038-1046.

55 Y. Nibu, R. Marui and H. Shimada, *Journal of Physical Chemistry A*, 2006, **110**, 9627-9632.

56 G. Herzberg, *Molecular Spectra and Molecular structure II*, 1945, Van Nostrand Reinhold: New York.

57 U. Samuni, S. Kahana and E. Haas, *Journal of Physical Chemistry A*, 1998, **102**, 4758-4768.

58 Y. Haas and U. Samuni, *Progress in Reaction Kinetics and Mechanism*, 1998, **23**, 211-280.

59 M. Y. Choi, G. E. Douberly, T. M. Falconer, W. K. Lewis, C. M. Lindsay, J. M. Merritt, P. L. Stiles and R. E. Miller, *International Reviews in Physical Chemistry*, 2006, **25**, 15-75.

60 I. Tolbatov, P. Bartl, J. Yurkovich, P. Scheier, D. M. Chipman, S. Denifl and S. Ptasinska, *Journal of Chemical Physics*, 2014, **140**, 034316.

61 *Physical Methods in Heterocyclic Chemistry, Volume 1- Nonspectroscopic Methods*, edited by A. R. Katritzky 1963, Academic, New York.

62 T. D. Klots, P. Devlin and W. B. Collier, *Spectrochimica Acta Part A-Molecular and Biomolecular Spectroscopy*, 1997, **53**, 2445-2456.

63 N. Sundaraganesan, S. Ilakiamani, P. Subramani and B. D. Joshua, *Spectrochimica Acta Part a-Molecular and Biomolecular Spectroscopy*, 2007, **67**, 628-635.

64 S. Mohan, N. Sundaraganesan and J. Mink, *Spectrochimica Acta Part A-Molecular and Biomolecular Spectroscopy*, 1991, **47**, 1111-1115.

65 M. M. Cordes and J. L. Walter, *Spectrochimica Acta Part A-Molecular Spectroscopy*, 1968, **A 24**, 1421-1435.

66 A. Suwaiyan, R. Zwarich and N. Baig, *Journal of Raman Spectroscopy*, 1990, **21**, 243-249.

67 R. Infante-Castillo, L. A. Rivera-Montalvo and S. P. Hernandez-Rivera, *Journal of Molecular Structure*, 2008, **877**, 10-19.